Spatial Organization of Immobilized Multienzyme Systems Improves the Deracemization of Alkyl Glyceryl Ethers.

Daniel A. Grajales-Hernández[a], Eleftheria Diamanti[a], Riccardo Moro[a], Susana Velasco-Lozano[b,c], Elisabet Pires[b], Fernando López-Gallego[a,c,d].*

[a]Heterogeneous biocatalysis laboratory, Center for Cooperative Research in Biomaterials (CICbiomaGUNE) - Basque Research and Technology Alliance (BRTA) Paséo Miramón, 194, 20014 Donostia-San Sebastián, Spain.

[b]Catálisis Heterogénea en Síntesis Orgánicas Selectivas, Instituto de Síntesis Química y Catálisis Homogénea (ISQCH-CSIC), University of Zaragoza, Pedro Cerbuna, 12, Zaragoza, Spain

[c]Aragonese Foundation for Research and Development (ARAID), 50018, Zaragoza, Spain

[d]IKERBASQUE, Basque Foundation for Science, Maria Diaz de Haro 3, 48013 Bilbao, Spain

KEYWORDS: biocatalysis, enzyme cascades, dehydrogenases, NADH, protein immobilization.

ABSTRACT

Production of enantiomerically pure molecules is of utmost importance in the pharma industry. In this context, biocatalysis emerges as an alternative to conventional chemical methods due to the exquisite selectivity and specificity underlying the enzymes. In this work, we design a multienzymatic system to perform the deracemization of alkyl glyceryl ethers as potential building blocks for the synthesis of drugs. The key to success in this route is controlling the spatial organization of the enzymes involved in the cascade through their immobilization on porous carriers. By fine-tuning the intraparticle organization of an enzymatic cascade comprising an (*S*)-selective glycerol dehydrogenase from *Bacillus stearothermophilus* and (*R*)-selective ketoreductase from *Lactobacillus kefir*, we performed the oxidoreductive deracemization of *rac*-alkyl/aryl glyceryl ethers with a yield up to 100% and enantiomeric excess, *e.e.* > 99%, otherwise impossible using a soluble system. Remarkably, we find that optimal spatial assembly of the biocatalyst ameliorates the inhibition phenomena experimented by the system and increases the deracemization rate by 4-fold. Finally, integrating an enzymatic NAD^+ regeneration system to the heterogeneous biocatalyst, we intensified the process by reusing it in discontinuous and consecutive batch cycles and scaling the reaction up to 250 mM substrate, achieving 100% yield and *e.e.* > 99%.

INTRODUCTION

Current chem and pharma industry tendencies seek to develop more sustainable processes and strategies to obtain building blocks and precursors for a broad gamma of drugs.[1] In this sense, the assembly of multienzyme systems performing reaction cascades in one pot stands out as one of the most successful approaches for this purpose. These enzymatic systems offer great specificity and selectivity, leading to high product yields in enantioselective procedures, with fewer by-products under mild reaction conditions.[2, 3] Nonetheless, this strategy represents a series of challenges, such as enzyme compatibility, stability, cross-reactivity, and inhibition due to the formation of intermediaries.[4] To tackle some of those disadvantages, multi-enzyme co-immobilization is a suitable approach that confines several enzymes in the same limited space, which often stabilizes them.[5-8] Furthermore, tailoring the colocalization of enzymes within the same solid porous particles allows optimal assembly of enzyme cascades, enabling substrates and intermediaries to be sequentially delivered to the next enzyme active as occurs in the cellular milieu, minimizing side reactions or toxicity of intermediates among other phenomena.[9]

Previous observations by our group have confirmed that intraparticle spatial organization by site-directed immobilization of each enzyme in a cascade is fundamental to carrying out biotransformations with relevant yields.[10, 11] To the best of our knowledge, the application of this kind of rational immobilization is null regarding cascades for the deracemization of molecules.

Enzymatic deracemization usually is performed in a two-stage cascade starting from a racemate; 1) the transformation of one or both enantiomers into a prochiral intermediate, and 2) transformation back into the stereocomplementary substrate molecule, now optically pure.[12] This process enables the transformation of 100% of the molecules into one enantiomer, in contrast to the 50% obtained in kinetic resolutions.[13] A nice example is described by the group of Kroutil.[14]

for the deracemization of secondary alcohols (**Scheme 1A**). Here, starting from a racemate, the undesired enantiomer is transformed into a prochiral ketone by selective oxidation, and in the second step, the ketone is asymmetrically reduced back into the secondary alcohol but in the desired configuration. Although other works have exploited similar approaches, none has exploited the potential of immobilization and spatial organization of enzymes on solid carriers in enzyme deracemization.[15, 16]

In this sense, alkyl glyceryl ethers (AGEs) are an interesting case of study, since their racemates are green solvents while their pure enantiomers are building blocks for several approved and commercial drugs (**Scheme 1B**).[17,18] Due to the presence of two hydroxyl groups in AGEs, this deracemization process is a chemical challenge because one needs to use enantio- and regioselective catalysts. To access optically pure AGEs, we previously designed a kinetic resolution, by engineering the active site of a glycerol dehydrogenase of *Bacillus stearothermophilus* (BsGlyDH variant L252A) allowing the position of AGEs into the active cavity.[18] This enabled the selective oxidation of the (*S*)-enantiomer into the corresponding alkyl hydroxyketone, yielding 50% product and 99% enantiomeric excess (*e.e.*) of (*R*)-AGEs. Nonetheless, inspired by the strategy used by Kroutil´s group,[14] this work pursues accessing 100% yield by coupling a second chemo- and enantioselective oxidoreductase, to achieve the stereoinversion of the (*S*)-enantiomer. For this purpose, the enzymes comprising such a two-step cascade can be co-immobilized and spatially organized to increase the reaction rate, minimize the accumulation of intermediaries, and increase the system stability.

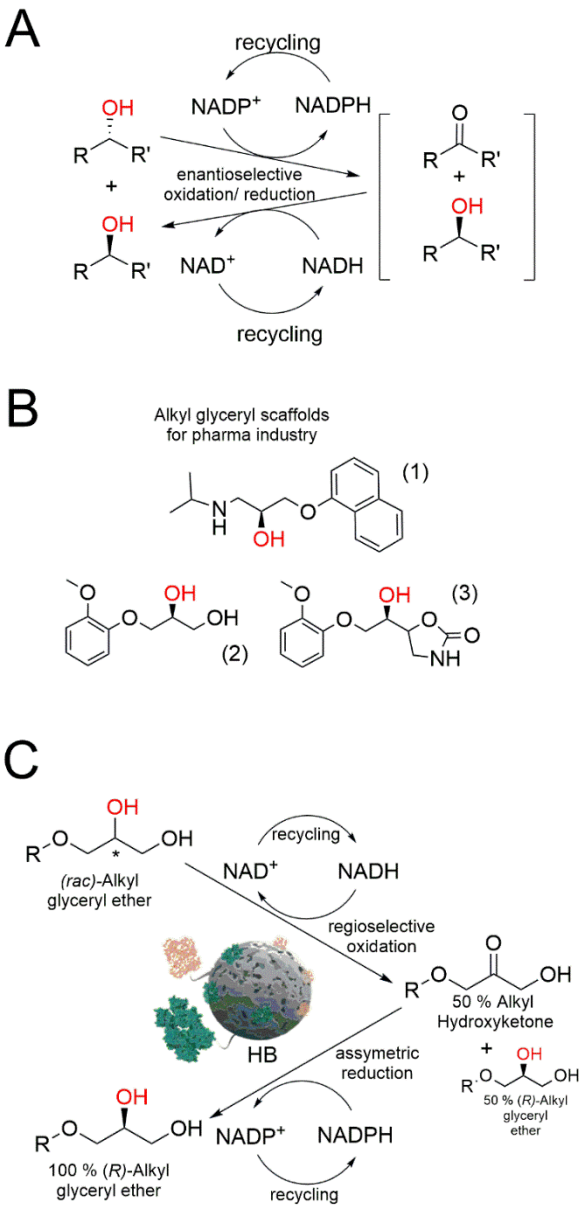

Scheme 1. Enzymatic strategies for the deracemization of molecules via oxidoreductive stereoinversion. A. Strategy employed by the group of Kroutil[14] for the deracemization of secondary alcohols. B. Most common enantiopure alkyl glycerol scaffolds employed in the pharma industry, (1) Propanolol, (2) Guaifenesin, (3) Mephenoxalone C. Designed strategy in this work for the deracemization of alkyl/aryl glyceryl ethers using a multienzymatic heterogeneous biocatalysts (HB).

The spatial organization of immobilized enzymes on porous supports can be modulated by modifying the immobilization kinetics of each enzyme.[19] As protein immobilization often takes place at higher rates than protein diffusion, the protein is mainly immobilized at the outer surface

of the porous particles. Nonetheless, by controlling the surface-protein interactions using competitors, the immobilization slows down, which lets enzymes diffuse and colonize the inner regions of the carrier.[19] In the search for the optimal spatial organization of multi-enzyme systems that allows substrates and intermediaries to meet enzymes in the proper order, we can tune the immobilization rate of the enzymes to control their location inside the carrier.[10]

Through this approach, we fabricated a spatially organized multienzyme heterogeneous biocatalyst to perform the deracemization of alkyl/aryl glyceryl ethers (AGE) via a two-step oxidoreductive stereoinversion. First, (*S*)-AGE from a racemate is oxidized into its corresponding hydroxyketone using the BsGlyDH-L252A variant, followed by the asymmetric reduction of that hydroxyketone back into AGE in its (*R*) configuration using a second (*R*)-selective ketoreductase (**Scheme 1C**). An optimal enzyme spatial configuration significantly increases the deracemization rate by decreasing the transient intermediate concentrations. Finally, we co-immobilized a cofactor regeneration system (NADH oxidase) together with the deracemization enzyme cascade for process intensification.

RESULTS AND DISCUSSION

Enzyme selection to assemble the deracemization cascade.

As a proof of concept, we designed a one-pot two-step enzymatic deracemization cascade via oxidoreductive stereoinversion to access (*R*)-ethyl glyceryl ether (EGE) as a model product. The first step consists of the regio- and enantio- selective oxidation of the (*S*)-ethyl glyceryl ether ((*S*)-EGE) from a racemate to ethyl hydroxyketone (EHK; 1-ethoxy-3-hydroxypropan-2-one), catalyzed by an engineered BsGlyDH-L252A previously developed in our lab. In the second step, an (*R*)-selective ketoreductase (KRED) is needed to asymmetrically reduce the hydroxyketone intermediate to the corresponding (*R*)-EGE. Using EHK as substrate, we first tested 4 different ketoreductases, from *Neurospora crassa* (NcKRED), *Candida glabratta* (CgKRED), *Bacillus subtilis* (BsKRED) and *Lactobacillus kefir* (LkKRED).[20-23] All tested enzymes were capable of reducing the carbonyl group of EHK, yet none oxidized ethyl glyceryl ether (EGE) under the presence of $NAD(P)^+$.

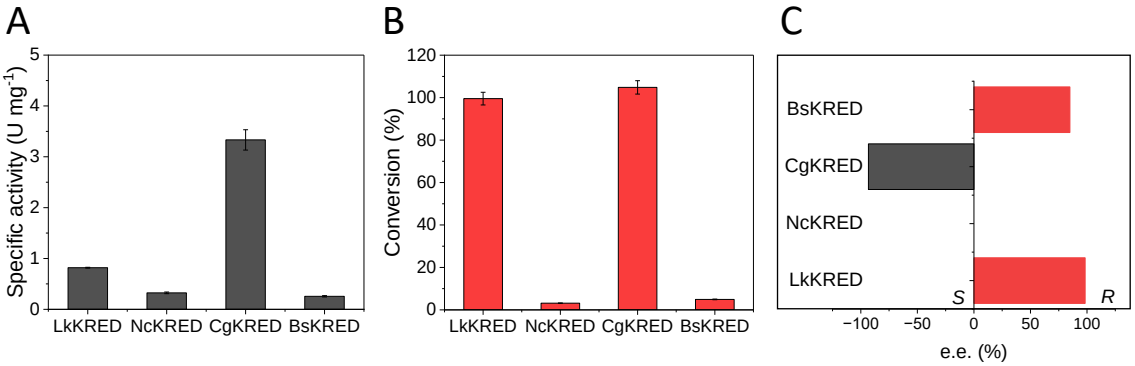

Figure 1. Selection of ketoreductases (KRED) for the conversion of 1-ethoxy-3-hydroxypropan-2-one (EHK) to (*R*)-ethyl glyceryl ether (*R*-EGE). A) Specific activity of different KREDs using 25 mM EHK and 0.5 mM NADPH at pH 7 and 25 ºC. B) Enzymatic conversion of EHK to 25 mM EGE after 24 h employing isopropanol for cofactor regeneration at pH 7 and 25 ºC. C) Enantiomeric excess (*e.e.*) of EGE after KRED-mediated EHK reductions shown in panel B.

Thus, the high chemoselectivity of KREDs guarantees the absence of reverse reactions that may limit the final yield of the process. **Figure 1A** shows that CgKRED is 4 to 13-fold more active

than the other KREDs herein tested. Next, we evaluated the ability of KRED to enantioselectively produce the (*R*)- enantiomer. To that aim, we performed the full reduction of the EHK (25 mM) and assessed both yield and *e.e.* of EGE (**Figure 1B-C**). As all tested KREDs employ NADPH, we use their capacity to oxidize isopropanol into acetone to *in situ* regenerate the cofactor. LkKRED and CgKRED quantitatively reduced EHK into EGE in 48 h, but only LkKRED achieved 99% *e.e.* of the *R*-configuration. BsKRED also produced (*R*)-EGE, but yields were less than 5% under the same conditions, thus we discarded this enzyme for further studies. Therefore, we selected LkKRED to be combined with BsGlyDH-L252A for the deracemization of EGE. The enantiopreference of LkKRED we found here matches with the enantioselectivity previously reported for this enzyme in the production of secondary alcohols.[23] Surprisingly, CgKRED offered an inverse configuration to that reported previously for ketones with small substituents. Hence, we suggest that the ether moiety of EHK induces some steric hindrances that pose this substrate within the active site of CgKRED in an inverted spatial configuration compared with less bulky ketones.[21]

Enzymatic deracemization of EGE through a two-enzymes cascade

We started evaluating the efficiency of the cascade using free enzymes according to the scheme shown in **Figure 2A**. Soluble LkKRED (1 mg mL^{-1} of reaction) was mixed with BsGlyDH-L252A (1 mg mL^{-1}) and the NAD^+ regeneration system composed of *Thermus thermophilus* NADH oxidase (TtNOX)[24] and bovine liver catalase (CAT).[25, 26] The NADPH required by LkKRED was self-recycled by the same enzyme in the presence of isopropanol through the Meerwein–Ponndorf–Verley (MPV) reduction reaction.[27] Using a BsGlyDH-L252A:LkKRED:TtNOX: CAT mass ratio of 1:1:1.6:0.4, which means an activity ratio of 1:0.25:10:1000, the soluble system only achieves an *e.e.* (*R*) = 42% (**Figure 2B**).

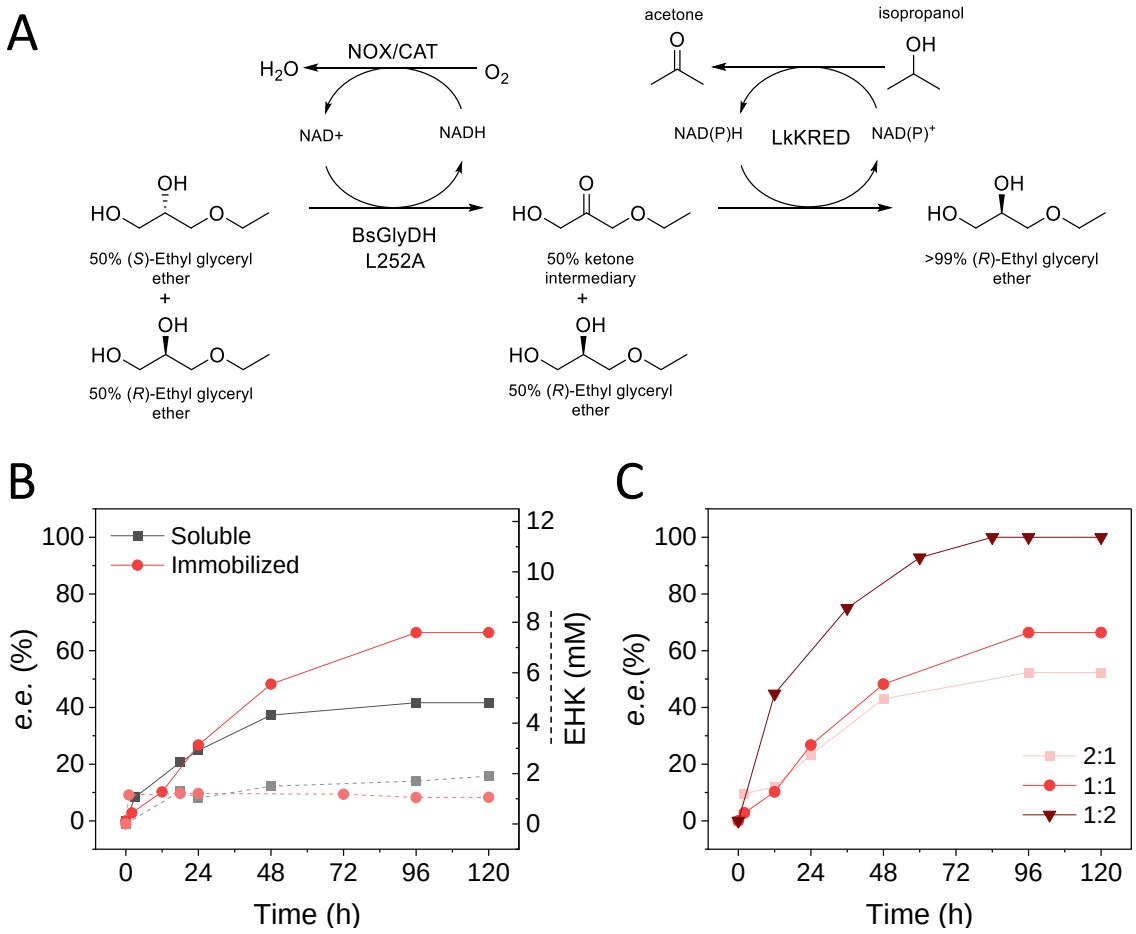

Figure 2. Deracemization of *rac*-EGE to R-EGE. A) Reaction scheme of the enzymatic deracemization of ethyl glyceryl ethers. B) Time-courses of *e.e.* progression (continuous line), and EHK production (dashed line), using soluble and immobilized enzymes with BsGlyDH-L252A/LkKRED mass ratio of 1:1 in reaction. C) Time-courses of EGE deracemization catalyzed by independently immobilized enzymes at different mass ratios in reaction. BsGlyDH-L252A/LkKRED mass ratios are colored in different grades of red. Reaction conditions: 25 mM *rac*-EGE, 1 mM NAD^+, 0.5 mM NAD(P)H, 150 µM FAD^+, and 15% isopropanol, at pH 7.0 and 25ºC. Soluble NAD^+ recycling system TtNOX/CAT was added in all reactions (the unit ratio is 1:10:1000 BsGlyDH:TtNOX: CAT).

In this cascade, the *e.e.* value is intimately linked to the product yield, which means that the two free enzymes working in tandem were capable of inverting only 5 mM (*S*)-EGE into (*R*)-EGE and accumulating 2 mM EHK, resulting in a 56% conversion but 40% product yield. The plateau in the reaction course indicates that either or both redox steps are halted, probably due to inactivation or inhibition issues underlying one or both free enzymes. As enzyme immobilization is a recurrent strategy to increase the stability of the enzyme systems,[28] we decided to separately immobilize

His-tagged BsGlyDH-L252A and LkKRED on porous agarose microbeads functionalized with Co^{+2}-chelates (AG-Co^{+2}) through their genetically fused His-tags that selectively interact with the cobalt chelates at the support surface. BsGlyDH-L252A and LkKRED were quantitatively immobilized on this support, however, the immobilized enzymes only recovered 5 and 28% of their initial activities, respectively (**Table S1**). The low recovered activity upon the immobilization of BsGlyDH-L252A matches our previous studies and can be attributed to the dissociation of its octameric quaternary structure.[18,29] To avoid dissociation of quaternary structure, several strategies have been proposed, such as the use of polyfunctional polymers such as dextran aldehyde,[29] or adding competitive inhibitors.[30] Furthermore, the high K_M of free BsGlyDH towards EGE (233mM) leads to rather low activities under assay conditions (25 mM).[18] This scenario is more dramatic for the immobilized enzymes since diffusional restrictions tend to increase the apparent K_M value, explaining the apparent reduction in recovered activity.[31]

Despite the reduced specific activity of the immobilized enzymes, we mixed these two heterogeneous biocatalysts to assess the deracemization of 25 mM *rac*-EGE to (*R*)-EGE in the presence of 15% isopropanol, 1 mM $NAD^{+,}$ and 0.5 mM NADPH, adding soluble TtNOX and CAT in mass ratio of 1:1:1.6:0.4 (BsGlyDH-L252A: LkKRED:TtNOX:CAT). Under these conditions, we achieved *e.e.* (*R*) = 66% after 120 h, accumulating low amounts of EHK (< 2 mM) (**Figure 2B**) and outperforming the system in solution despite the 4-20 times lower specific activities of immobilized enzymes. The accumulation of the hydroxyketone may be responsible for the suboptimal performance of the cascade as BsGlyDH, but also its variant BsGlyDH-L252A, suffer product inhibition.[18]

Encouraged by these results, we optimized the mass ratio between BsGlyDH-L252A and LkKRED to maximize the throughput of the cascade. To this aim, we tested three different BsGlyDH-

L252A: LkKRED mass ratios; 2:1, 1:1, and 1:2, keeping a BsGlyDH-L252A load of 10 mg $g^{-1}_{support}$ (**Figure 2C**). Using a mass ratio of 1:2, we achieved 100% product yield with *e.e.* (*R*) > 99% after 120 h, detecting no EHK intermediate. ^{1}H-NMR and COSY analyses show that the deracemized product presents the same spectrum as the racemic substrate, demonstrating that the deracemization cascade does not alter the chemical structure of EGE but its enantiomeric configuration (see supporting information, **Figure S1-S2**). In contrast, when BsGlyDH-L252A is equal or in excess regarding LkKRED, we detect 0.5-1 mM EHK during the reaction course (**Figure S3**). Thus, the excess of LkKRED prevents the accumulation of EHK, which may minimize the product inhibition that BsGlyDH-L252A undergoes, thereby increasing the overall deracemization rate. Hence, we report a heterogeneous biocatalytic system for the regioselective deracemization of diol racemates via an oxidoreductive stereoinversion cascade that outperforms other previously described enzymatic and chemoenzymatic systems for the oxidoreductive stereoinversion of 1-phenyl-1,2-ethanediol (95% yield *e.e.* = 92%)[16] and allyl glyceryl ethers (68% yield, *e.e.* = 75%),[32] respectively. In these last two examples yields and *e.e.* are inferior to those found in this work and did not resort to the use of immobilized biocatalysts with reusability potential.

Next, we optimized the BsGlyDH-L252A concentration in the reaction keeping constant the BsGlyDH-L252A: LkKRED mass ratio to 1:2 (**Figure S4**). Surprisingly, we observe similar deracemization rates, product yields, and *e.e* (*R*) values with no accumulation of EHK regardless of the enzyme concentration in reaction, pointing out other parameters controlling the deracemization rate. We hypothesize that mass transport restrictions suffered by the intermediate (EHK) to travel from one immobilized biocatalyst (BsGlyDH-L252A) to the other (LkKRED)

dominate the deracemization rate, rather than the intrinsic enzyme kinetics of the immobilized enzymes.

Optimizing the spatial organization of immobilized bi-enzyme systems to enhance the deracemization performance.

To demonstrate the hypothesis proposed in the previous section, we co-immobilized both His-tagged BsGlyDH-L252A and LkKRED on the same particle of AG-Co^{2+} but with different intraparticle spatial organizations, using the optimal 1:2 mass ratio at the lowest enzyme BsGlyDH load (10 mg $g^{-1}_{support}$). Mass transport restrictions underlying EHK can be dramatically altered depending on the relative position of the two enzymes across the porous surface of the support, as such intermediate can diffuse from one enzyme to the other without abandoning the porous particle where it has been generated, which may ultimately improve the deracemization rate. To achieve different spatial patterns of the two enzymes within each porous agarose bead, we co-immobilized both enzymes at different immobilization rates by adding a competitor that slows down the immobilization process.[10, 11, 19] While a high immobilization rate allows localizing enzymes at the outer surface of the porous beads as their diffusion is slower than their immobilization, slow immobilization permits enzymes to colonize the inner surface of the support as the protein diffusion equalizes with the immobilization. In the case of His-tagged enzymes, the use of imidazole at a high concentration slows down the immobilization rate, resulting in more uniform enzyme distributions across the bead porous surface. According to this, we propose 4 patterns of co-immobilized bi-enzyme systems and 1 pattern where both enzymes were immobilized on different beads (**Figure 3**, left panels).

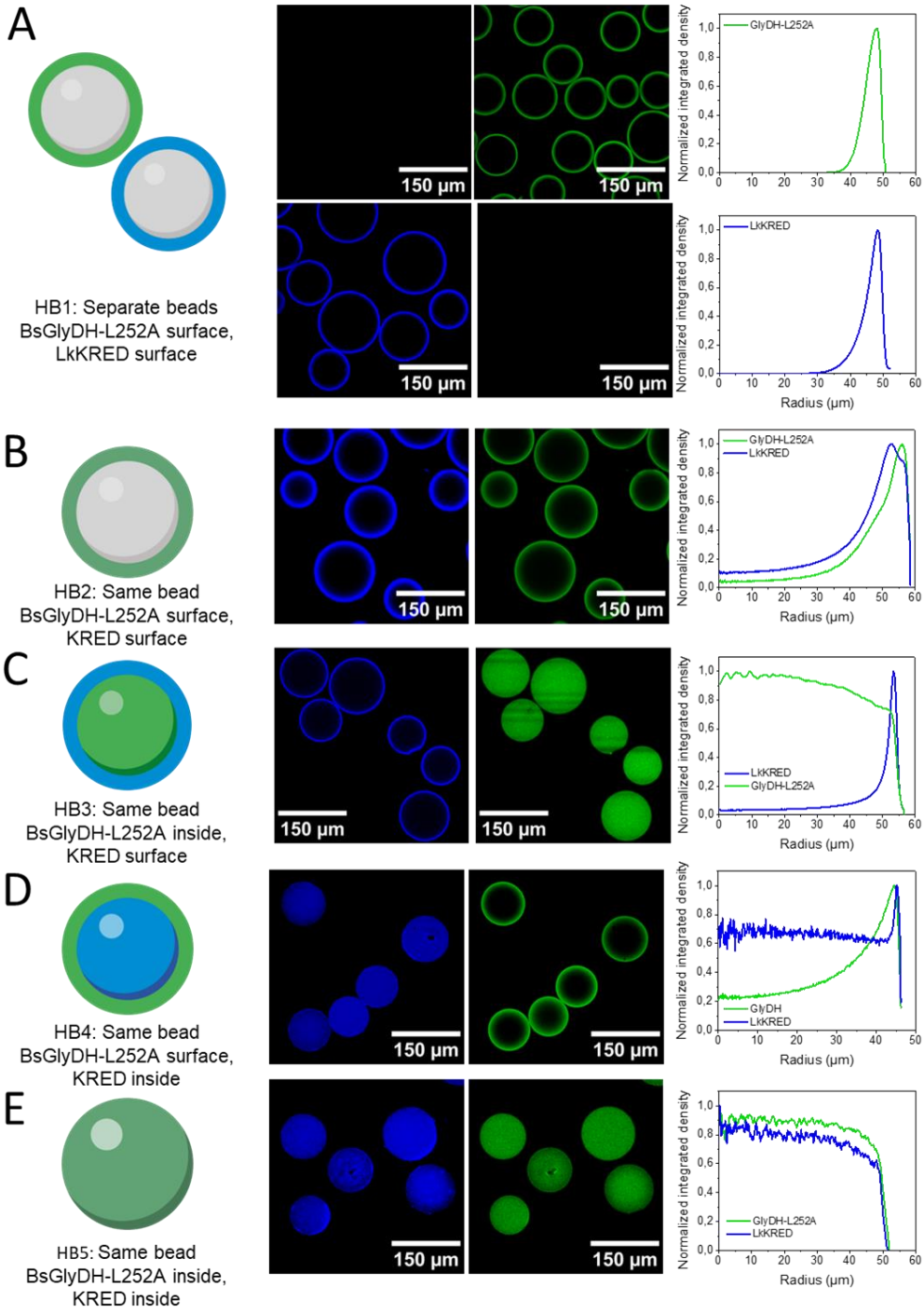

Figure 3. Evaluation of the spatial distribution for different heterogeneous biocatalysts (HB) where BsGlyDH-L252A and LkKRED are (co)immobilized on porous agarose microbeads. A) HB1, B) HB2, C) HB3, D) HB4 and E) HB5. Schemes (left-panels) and confocal laser scanning microscopy (CLSM) images (middle panels) of fluorescein isothiocyanate-labeled BsGlyDH-L252A (green channel, λex: 494 nm) and ATTO NHS-labeled LkKRED (blue channel, λex: 476 nm) (co)immobilized on AG-Co^{2+} carriers with different spatial distributions. For each spatial distribution, the radial profiles of the labeled enzymes immobilized on AG-Co^{2+} beads (n > 10) are provided (right panels).

These organization patterns were confirmed using labeled BsGlyDH-L252A and LkKRED with fluorescein isothiocyanate and ATTO 390 NHS ester, respectively. These fluorophore-labeled enzymes were immobilized under different conditions and analyzed through confocal laser scanning microscopy (CLSM; **Figure 3**, middle panels).

The average radial profile of different beads confirms the spatial organization patterns of five heterogeneous biocatalysts (HB1-5) (**Figure 3**, right panels). **Figure 3A** shows the HB1 spatial configuration where the two enzymes are localized at the outer surface of two different AG-Co^{2+} beads. **Figure 3B** shows the HB2 spatial configuration where both enzymes colocalize at the outer surface of the same bead as both enzymes are rapidly immobilized in the absence of immobilization competitors. **Figure 3C** shows the HB3 spatial configuration where BsGlyDH-L252A is first and slowly immobilized in the presence of 100 mM imidazole, positioning the enzyme uniformly across the bead, whereas LkKRED is then rapidly immobilized in the absence of imidazole locating it at the outer surface of the bead. **Figure 3D** shows the HB4 spatial configuration following the inverse immobilization sequence as HB3; LkKRED is first and slowly immobilized, whereas BsGlyDH-L252A is next immobilized very rapidly at the outer surface. Finally, **Figure 3E** shows the HB5 spatial configuration where both enzymes are co-immobilized in the presence of 100 mM imidazole and thus colocalize uniformly across the entire porous surface of the bead.

The different spatial patterns result in bi-functional heterogeneous biocatalysts with different immobilization parameters, including enzyme density and colocalization coefficients (**Table 1, Figure S5**). When enzymes are immobilized on the surface of the bead, (without competitors) their immobilization yields were 100%; these are the cases for BsGlyDH-L252A and LkKRED in HB1 and HB2, for BsGlyDH-L252A in HB4, and LkKRED in HB3. On the other hand, when the

Table 1. Immobilization parameters and colocalization coefficients of heterogeneous biocatalysts with different spatial organization.

Parameters	Enzyme	HB1	HB2	HB3	HB4	HB5
Immobilization yield (%)	BsGlyDH L252A	97	93	35	95	56
	LkKRED	94	93	92	72	56
Recovered Activity[1] (%)	BsGlyDH L252A	2.9	7.8	5.9	4.4	4.0
	LkKRED	17	17	14	15	17
Biocatalyst activity (U/g)	BsGlyDH L252A	0.4	0.9	0.8	0.55	0.5
	LkKRED	2.5	2.54	2.12	2.40	2.74
Density ($x10^8$) molecules μm^{-3}	BsGlyDH L252A	2.1	1.26	0.33	1.63	0.33
	LkKRED	1.6	0.92	3.35	0.41	0.40
Pearson Coeff	BsGlyDH L252A	NA	0.90	0.32	0.53	0.46
	LkKRED	NA	0.88	0.25	0.36	0.48
Manders Coeff	BsGlyDH[2] L252A	NA	93	35	95	56
	LkKRED[3]	NA	93	92	72	56

[1]Recovered activity is defined as the percentage of the specific activity of the immobilized enzyme regarding the specific activity of the free enzyme. The specific activity of the free enzymes is 1.3 and 0.81 U x mg^{-1} for BsGlyDHL252A and LkKRED, respectively. [2] Percentage of the BsGlyDH-L252A fluorescence signal that co-localizes in the same pixel with LkRED fluorescence signal. [3] Percentage of the LkKRED fluorescence signal that co-localizes in the same pixel with BsGlyDH-L252A fluorescence signal.

enzyme immobilization is slowed down in the presence of imidazole, the immobilization yields were near 50% (BsGlyDH-L252A in HB3, LkKRED in HB4, and both enzymes in HB5). In these cases, we matched the optimal mass ratio BsGlyDH-L252A: LkKRED to 1:2 by increasing the enzyme concentration offered in the immobilization process, achieving a BsGlyDH-L252A and LkRED loadings of 10 and 20 mg $g^{-1}_{support}$, respectively. In all cases, the recovered activities of immobilized BsGlyDH-L252A and LkRED range from 3-8% and 14-17%, respectively. These

values are similar to those obtained for the two enzymes immobilized individually on the same support with similar protein loads (HB1).

With the different heterogeneous biocatalysts in hand, we studied the effect of the enzymes' spatial organization on the deracemization efficiency by quantifying the rate, product yield, *e.e.* (*R*), and intermediate accumulation (**Figure 4**). In all cases, we achieved *e.e* (*R*)> *99%* but found differences in the deracemization rates and EHK accumulation among the heterogeneous biocatalysts. **Figure 4A** shows that HB3 deracemizes *rac*-EGE between 2.2 to 3.6 times faster than the rest of the HBs. While HB1-2 and HB 4-5 need 96 h to complete the deracemization process, HB3 only requires 24 h to reach an *e.e.* (*R*) > 99%. Hence, we suggest that the transport of the intermediate is maximized when LkKRED localizes at the outer surface, whereas BsGlyDH-L252A is located throughout the entire bead. In this spatial pattern, both enzymes only colocalize in the outermost 5 µm of the bead radius. When both enzymes are immobilized on two different beads, HB1 exhibits a similar deracemization rate as HB2 and HB5 where both enzymes are co-immobilized and co-localized onto the same beads.

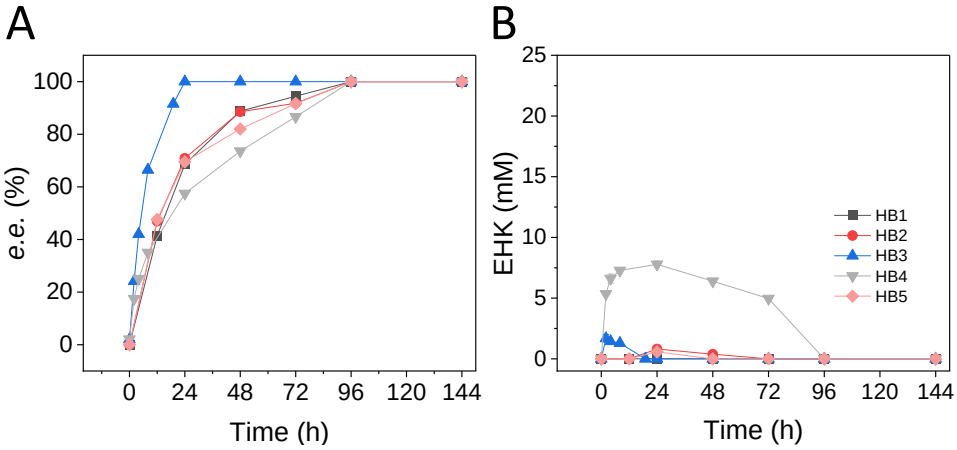

Figure 4. Time-courses of the EGE deracemization driven by heterogeneous biocatalysts with different spatial organizations. A) Enantiomeric excess as a function of the reaction time. B) EHK accumulation as a function of the reaction time. Reaction conditions: 25 mM *rac*-EGE, 1 mM NAD^+, 0.5 mM NAD(P)H, 150 µM FAD^+, and 15% isopropanol, at pH 7.0 and 25 ºC. Soluble NAD^+ recycling system TtNOX/CAT was added in all reactions (the unit ratio is 1:10:1000 BsGlyDH:TtNOX: CAT).

In the case of HB2, both enzymes co-localize at higher protein densities than in HB5 with opposite spatial configurations (**Table 1, Figure S5**). As these three heterogeneous biocatalysts deracemize EGE with similar efficiencies, we conclude that neither enzyme density nor enzyme colocalization within the same bead alone can explain the acceleration of the deracemization cascade. More intriguing is the fact that HB4 is the slowest heterogeneous biocatalyst, presenting a spatial distribution opposite to that found for HB3. This result is explained by the high accumulation of EHK detected in the process catalyzed by HB4 (>7 mM EHK at roughly 30% substrate conversion; **Figure 4B**). Thus, to maximize the deracemization rate both dehydrogenases must be co-immobilized on the same bead but with different intraparticle enzyme distributions where a very dense layer of LkKRED is located at the outer surface of the beads and BsGlyDH-L252A occupies the interior surface at lower protein density.

Unveiling the cause of EHK accumulation in the system.

The differences in the deracemization efficiency we found between HB3 and HB4 led us to interrogate more in-depth these two systems. One possible explanation for these differences may be the high concentration of EHK accumulated with HB4, pointing out an inhibitory effect of this intermediate over BsGlyDH-L252A as reported elsewhere for other hydroxyketones.[18, 25] BsGlyDH-L252A inhibition studies confirmed that EHK is a potent inhibitor for this enzyme variant with a half maximum inhibitory concentration (IC_{50}) < 0.5 mM (**Figure S6**). Although this variant was less inhibited by EHK than the wild-type enzyme, the alkylated hydroxyketone was a better inhibitor than dihydroxyacetone (DHA).

If BsGlyDH-L252A is inhibited by the accumulated EHK during the deracemization process, the NAD^+ recycling will cease. To test this hypothesis, we first compared the recycling efficiency of

NAD^+ (which is exclusively linked to the first step of the reaction) in HB3 and HB4 by monitoring the H_2O_2 production rate using a peroxidase-coupled colorimetric assay (**Figure 5A** and **Scheme S1**).[33, 34] Each mol of NADH oxidized to NAD^+ by TtNOX generates one mol of H_2O_2, therefore the production of the latter reflects the recycling of that nicotinamide cofactor. **Figure 5A** shows that the formation of H_2O_2 stops after 5 minutes when using HB4, while HB3 constantly produces H_2O_2 along the assay. This behavior indicates that the NAD^+ recycling is halted using HB4 and supports the early inhibition of BsGlyDH-L252A when EHK is transiently accumulated in the bulk under this enzyme spatial organization. In contrast, HB3 maintains the ongoing regeneration of NAD^+ because nascent EHK is efficiently reduced by the well-positioned LkKRED, preventing its accumulation. Hence, the process catalyzed by HB3 never reaches inhibitory concentrations of EHK, in contrast to what we observe with HB4 where the first oxidative step is paused until LkKRED reduces EHK, depleting it to non-inhibitory concentrations. These results suggest the existence of different intraparticle EHK concentration gradients within HB3 and HB4 due to the different spatial configurations of these heterogeneous biocatalysts. To evaluate the differences in EHK concentration inside HB3 and HB4 during the deracemization process, we designed an experimental proceeding to quantify the intraparticle EHK concentration (**Figure 5B**). After 2 h of deracemization reaction, the heterogeneous biocatalysts were separated from the reaction bulk and washed with distilled water in a 1:1 (w:v) ratio. Both bulk and washed samples were analyzed by GC-FID to determine the concentration of EHK inside and outside of the microbeads. In HB3, we find a 0.017 mM EHK inside the microbeads, while no EHK is detected in the reaction bulk, strongly suggesting that the reaction rate of the second step (LkKRED) exceeds the diffusion rate,[35] limiting the EHK diffusion out of the microbead (**Figure 5C**). On the other hand, we found 0.14 mM and 2.7 mM EHK inside the microbeads of HB4 and in the bulk, respectively (**Figure 5C**),

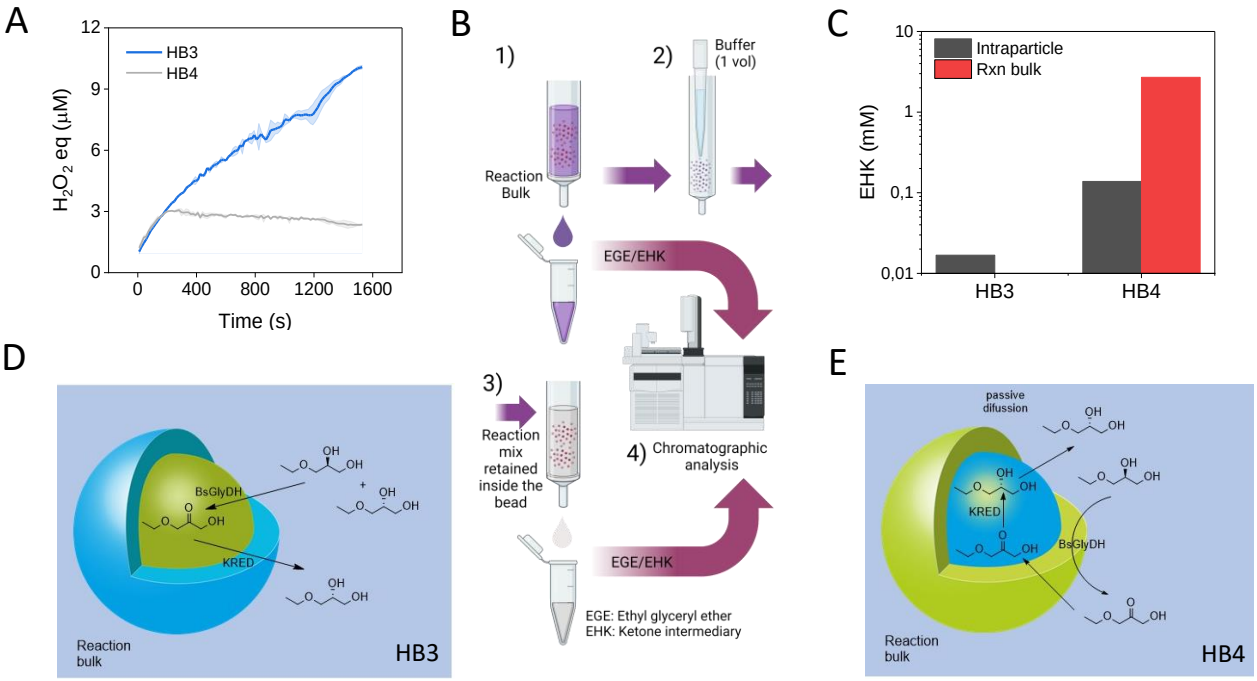

Figure 5. Effect of EHK accumulation on the deracemization of EGE. A) Monitoring of H_2O_2 production associated with NADH production in HB3 (blue) and HB4 (grey). B) Methodological scheme to quantify the intraparticle and bulk concentrations of EHK during the deracemization reaction. 1) Recovery of the reaction bulk. 2) Buffer washing of HBs to remove intraparticle EHK. 3) Recuperation of intraparticle EHK resuspended in buffer. 4) Chromatographic analysis of EHK. C) EHK intraparticle concentration (black) and concentration found in the reaction bulk (red). D-E) Proposed diffusion pathways of EHK during the deracemization cascade catalyzed by HB3 (D) and HB4 (E).

suggesting that the diffusion of EHK to the surroundings of LkKRED (located inside the microbeads) is limited.

When using HB3, the intraparticle EHK concentration is higher than that in the bulk, creating an outwards EHK gradient that pushes the produced intermediate out of the microbead and far from the inner BsGlyDH-L252A, mitigating its inhibition. Moreover, this diffusion pathway obligates EHK to cross an outer dense layer of LkKRED (3.35 x10^8 molecules µm^{-3}), which is 10.2 times more crowded on the outer surface than BsGlyDH-L252A inside the microbeads (**Figure 5D** and **S2**). Contrarily, HB4 creates an inwards EHK gradient as its concentration in the bulk is 20 times higher than inside the biocatalysts´ microbeads, forcing this intermediate to cross a dense layer of BsGlyDH-L252A (1.63 x10^8 nmol µm^{-3}) before reaching its target enzyme LkKRED, located

inside the microbeads (**Figure 5E**). This diffusion pathway submits BsGlyDH-L252A to a high concentration of EHK, inducing its inhibition before LkKRED can reduce that intermediate.

Scope of the enzymatic deracemization with HB3.

Based on our previous results, BsGlyDH-L252A can oxidize a broad scope of alkyl ethers with the same enantioselectivity observed for EGE[18]. Therefore, we assessed HB3 for the deracemization of several alkyl and aryl glyceryl ethers to assess the scope of this heterogeneous biocatalyst.

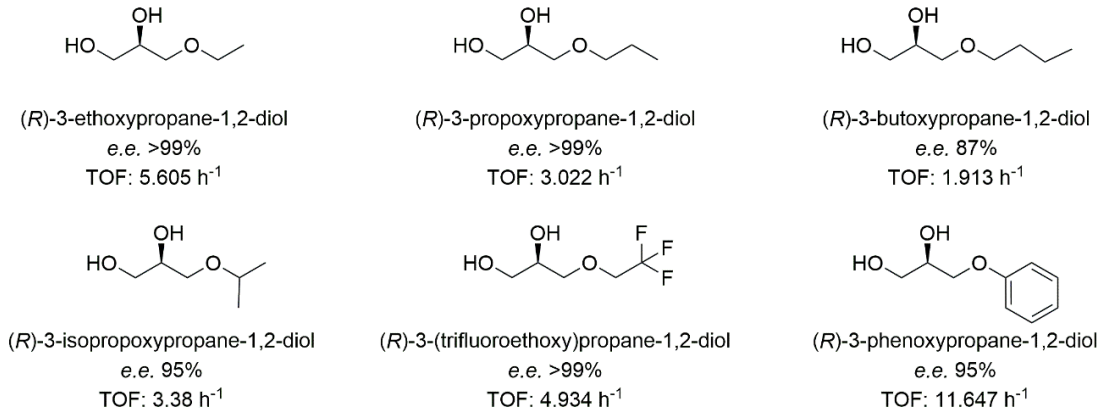

Figure 6. The substrate scope of HB3 for the deracemization of various alkyl and aryl ethers of glycerol. TOF: Turnover frequency is defined as the mol of product per mol of enzyme per hour before reaching *ee* > 40%. Reaction conditions: 25 mM *rac*-AGE, 1 mM NAD^+, 0.5 mM NAD(P)H, 150 µM FAD^+, and 15% isopropanol, at pH 7.0 and 25 ºC. Soluble NAD^+ recycling system TtNOX/CAT was added in all reactions (raio 1:10:1000 respect BsGlyDH units).

Using this heterogeneous biocatalyst coupled with soluble TtNOX and CAT, all substrates but butyl glyceryl ether (3-butoxypropane-1,2- diol) were deracemized with *e.e.* (*R*) >95% in less than 168 h (**Figure 6** and **S7-S9**). Only EGE was deracemized in less than 48 h, while interestingly, the most impeded and electronegative trifluorinated substrate 3-(trifluoroethoxy) propane-1,2- diol is the second best-deracemized substrate (72 h). This agrees with previously reported results where

this substrate is also oxidized efficiently due to the suitable shape and size of the active cavity of the BsGlyDH-L252A.[18] To note, the aryl glyceryl ether, 3-phenoxypropane-1,2-diol was deracemized very fast in the first 12 h with the highest TOF reported in this study, but the deracemization process slowed down afterward needing a total of 168 h to reach a maximum *e.e.* = 95%. Since all these transformations occur with yields superior to 50%, we can confidently affirm that LkKRED was able to reduce all intermediaries (1-alkoxy-3-hydroxypropan-2-ones). As for the case of EGE, ^{1}H-NMR analyses show that the deracemized product presents the same spectrum as the racemic substrate (**Figure S9**). Remarkably, HB3 is also able to complete the stereoinversion of (*S*)-EGE into (*R*)-EGE in 96 h (**Figure S10**).

One-pot chemo-enzymatic synthesis of optically pure *R*-isopropyl glyceryl ether.

Harnessing the potential of HB3 to perform the effective deracemization of the isopropyl glyceryl ether (iPGE), we propose the sequential chemoenzymatic synthesis of optically pure *R*- iPGE from glycidol and isopropanol, to address an integral process, skipping purification steps, minimizing wastes, and advancing the biorefinery concept. This is possible because the chemical synthesis of *rac*-iPGE offers a final reaction crude containing isopropanol,[17] the ancillary substrate required by LkKRED for the NADPH recycling. First, we performed the synthesis of *rac*-iPGE employing glycidol and an excess of isopropanol (1:15 molar ratio) using 20% mol NaOH as a catalyst. After a 2 h reaction, the preparation was cooled down and neutralized. Next, the reaction crude was diluted with the deracemization reaction mix (1 mM NAD^+, 0.5 mM NADPH, 0.15 mM FAD^+, 25 mM buffer sodium phosphate pH 7.0) to achieve a final concentration of 25 mM of *rac*-iPGE and leaving a total isopropanol amount near to 11% (v:v) in the final bulk (**Figure S11**). As a result, we achieved optically pure iPGE in 96 h with a 100% yield using HB3 as a biocatalyst. Here we

successfully achieved a sequential two-step, one-pot chemoenzymatic synthesis of optically pure *R*-isopropyl glyceryl ether, with minimal production of residues. Our group already proved the one-pot sequential synthesis and kinetic resolution of (*R*)-EGE using a reaction crude of EGE containing ethanol. The reaction yield was 40% with *e.e.* (*R*) = 90% due to the limitations of the biocatalysts and the kinetic resolution process.[18] Now, the optimized spatial distribution of HB3 allows us to reach the maximum yield and *e.e.* in an integral chemo-enzymatic process to transform racemic glycidol and isopropanol into enantiopure *R*-isopropyl glyceryl ether.

Assembling of the cofactor regeneration system, operational stability, and process intensification.

As the optimal spatial organization was found in HB3, we proceeded to immobilize the NAD^+ recycling enzymes to avoid the addition of free enzymes during the process and ultimately reuse the whole biocatalytic system. To this aim we explored two configurations of the NAD^+ recycling system; 1) water forming NADH oxidase from *Lactobacillus pentosus* (LpNOX) tagged with His-tag co-immobilized with HB3, which allows the oxidation of NADH to NAD^+ without forming H_2O_2,[36] thus skipping the use of CAT, and 2) a His-tagged TtNOx co-immobilized with HB3 combined with the untagged CAT separately immobilized on different support as HB3 since it lacks the needed His-tag to be immobilized on AG-Co^{+2}. In both configurations, NOX was aimed to be localized at the outer surface of the microbeads (immobilized without imidazole as a competitor) to maximize the O_2 diffusion.[11] In the first configuration, LpNOx was quantitatively immobilized on the outer surface of the same bead HB3 (HB3-LpNOx) retaining only 3.7% of activity (**Figure S12**). Using this heterogeneous biocatalyst, the deracemization stops at *e.e.* (*R*) = 50% after 24 h (**Figure S13**). Only when the loading of LpNOX was increased 5 times in HB3-LpNOX, we achieved the complete deracemization although it took 48 h, double the time than

using the TtNOX/CAT system in solution. No accumulation of EHK during the reaction indicates that LkKRED efficiently drives the reduction step, confirming the slowness of EGE oxidation due to an inefficient NAD^+ recycling system. We suggest that the low operational stability of LpNOx previously reported by our group hampers the deracemization process.[26] In contrast, the second configuration results in a heterogeneous biocatalyst HB3-TtNOX where His-tagged TtNOX recovers 4.4% of its initial activity upon the immobilization process. The auxiliary CAT was immobilized on agarose microbeads functionalized with glyoxyl groups (AG-G) with an immobilization yield of 36% and a recovered activity of 22%. When both heterogeneous biocatalysts are mixed, we obtained the fastest deracemization rate among all the systems herein studied. Having the dehydrogenases and the oxidases co-immobilized through their optimal spatial distribution and the catalase separated in a different particle the system is 4 times faster than the two dehydrogenases co-immobilized and combined with the free TtNOX/CAT system. As a result, the complete deracemization of EGE takes place in only 8 h with *e.e.* (*R*) > 99% and product yield of 97% yield (**Figure S13**).

Lastly, we tested the operational stability of the selected biocatalysts in sequential batch cycles (25 mM) at 24 h for the HB3-LpNOx system, and for 12 h for HB3-TtNOX mixed with CAT@AG-G (**Figure 7**). The *e.e.* is dramatically reduced after the first cycle using the former system, whereas the latter system reaches high *e.e.* 93% and 86 % product yield values after 3 consecutive batch cycles. Therefore, the superior operational stability of TtNOX is evidenced in this experiment, being the best option to intensify the process. To this aim, we either increased the substrate concentration or the reaction volume maintaining the biocatalyst volumetric load for the deracemization of EGE as a model substrate.

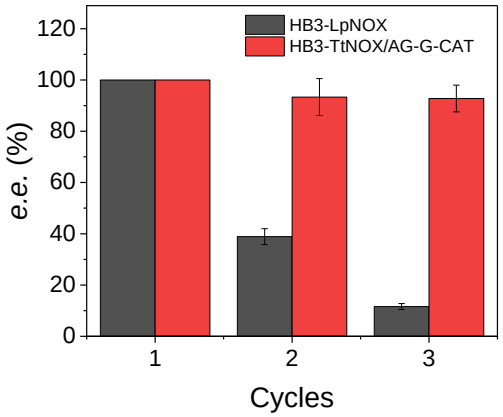

Figure 7. Comparison of the operational stability of the HB3-based biocatalysts integrating two different NADH oxidases as recycling systems. (Red) TtNOX plus catalase immobilized on a separate support AG-G. (Grey) LpNOX. Reactions were performed at 25 mM *rac*-EGE. Reaction conditions: 25 mM *rac*-EGE, 1 mM NAD^+, 0.5 mM NAD(P)H, 150 µM FAD^+, and 15% isopropanol, at pH 7.0 and 25 ºC.

We first scaled up the EGE concentration up to 500 mM (20x factor) using the optimal heterogeneous biocatalytic system described above (HB3-TtNOX) (**Figure 8A**). Expectedly, the deracemization rate increases along the substrate concentration, completing the process in less than 120 h using 250 mM of EGE. Only when using 500 mM, the complete deracemization was unafforded, reaching a maximum *e.e.* (*R*) =75%. The plateau observed in the deracemization process may be explained by the inhibition of the oxidative step as 17.8 mM EHK is transiently accumulated.

Secondly, we scale up the reaction volume 20-fold with 25 mM of EGE (**Figure 8B**) and 20% (w:v) biocatalysts load. Herein, we reach optically pure (*R*)-EGE in a period of 24 h with a yield of 100%. This process is slightly slower than that observed in the 1 mL reaction, where the same enantiopurity and yield were achieved after 8 h. We hypothesized that oxygen diffusional restrictions generated by changing the agitation and area/volume ratio of the larger volume reaction are responsible for this drop in the deracemization rate.

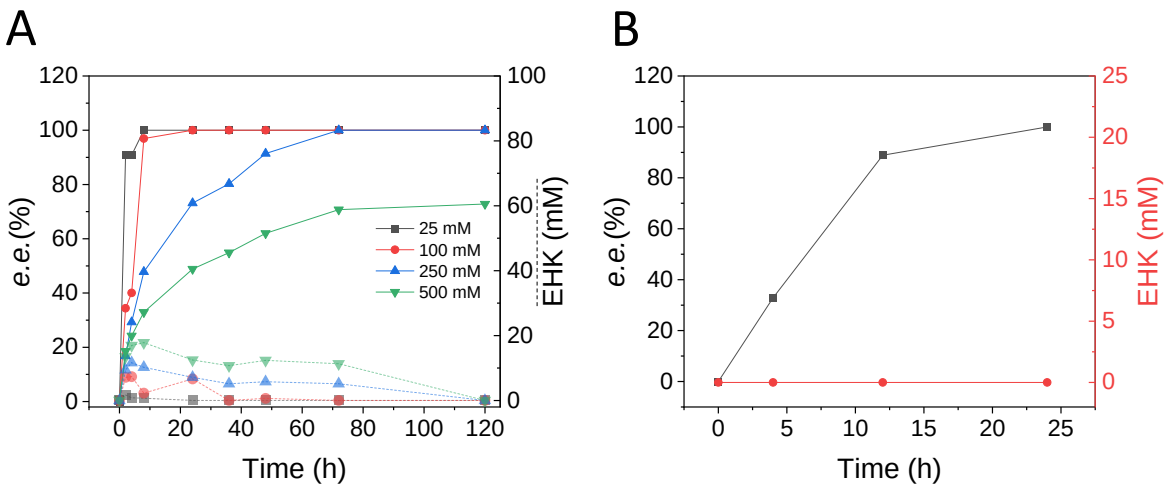

Figure 8. Intensification strategies for the EGE deracemization catalyzed by biocatalyst HB3-TtNOx/CAT@AG-G. A) intensification by increasing concentrations of substrate, from 25 (used in all previous assays) to 500 mM (increasing factor of 20), the continuous line shows the *e.e.*, while the dashed line shows the EHK production in each case. B) Intensification by increasing reaction volume by a factor of 20; the black line shows the enantiomeric excess, while the red line shows EHK production. In all cases, the volumetric load of the heterogeneous biocatalyst is kept at 20% (w:v).

By comparing the deracemization productivities in the path to intensification, we found that the best strategy is to increase initial concentrations of EGE, as volumetric productivity of 0.125 g L^{-1} h^{-1} is achieved using 250 mM substrate, which means a 2 times higher productivity than scaling the reaction volume using 25 mM substrate (0.06 mg L^{-1} h^{-1}). Furthermore, since using higher concentrations of the substrate increases the molar ratio substrate: enzyme, we found a specific productivity of 1.52 µmoles h^{-1} mg_{enzyme}^{-1}, 5-fold greater than that found by increasing the volume of the reaction (0.305 µmoles $h^{-1}mg_{enzyme}^{-1}$).

Conclusion.

The enzymatic deracemization of alkyl glyceryl ethers by a heterogeneous biocatalyst was achieved by designing and fabricating a multienzyme system meticulously arranged for a one-pot reaction. Assembling of a multifunctional heterogeneous biocatalyst comprising BsGlyDH-L252A

and LkKRED enzyme was able to perform the deracemization of EGE with an enantiomeric excess of 99% for the (*R*)-isomer. The spatial organization of the involved enzymes and the selection of the NAD^+-recycling enzyme are crucial for the performance in the deracemization, reducing the reaction time from 96 to 8 h. We find out that the reduction of the transient concentrations of EHK allows us to significantly reduce its inhibiting effect over BsGlyDH-L252A. Furthermore, integration of TtNOX/CAT in the heterogeneous biocatalytic system is very effective and allows for increasing the deracemization rate. Production of enantiomerically pure ethyl glyceryl ether employing the multi-functional heterogeneous biocatalyst herein made has a high potential for the synthesis of similar building blocks in pharmaceutical manufacturing, according to the current needs of greener synthetic approaches in the industry. This work exemplifies the valorization of a family of green solvents such as alkyl glyceryl ethers into pharmaceutical intermediates; a promising concept recently developed by Merck´s biocatalysis group transforming the bio-based solvent Cyrene into a precursor for the synthesis of Nemtabrutinib.[37]

METHODOLOGY

Materials

All chemicals and reagents employed here were purchased from Sigma Aldrich (St. Louis, IL, USA), except for those specified in the following sections. Cofactors Nicotinamide adenine dinucleotide reduced disodium salt (NADH), nicotinamide adenine dinucleotide sodium salt (NAD^+), Nicotinamide adenine dinucleotide phosphate reduced disodium salt (NADPH) nicotinamide adenine dinucleotide sodium salt ($NADP^+$), and isopropyl b-D-thiogalactopyranoside (IPTG), were purchased from GERBU Biotechnik GmbH (Wieblingen, Germany) Flavin adenine dinucleotide disodium salt was purchase from Cymit Química (Pamplona, Spain). *rac*-Ethyl glyceryl ether and pure enantiomers (*R*) and (*S*) of the same molecule, were synthesized and characterized as previously reported.[17] Cobalt-activated agarose microbeads 6BCL (AG-Co^{2+}) (particle size; 50 –150 mm, pore size; 112 nm and 15 mmol of Co^{2+} per g carrier) were purchased from ABT technologies (Madrid, Spain).

Enzyme production and purification.

All enzymes were obtained from synthetic genes cloned into pET28b (+) plasmids (aminoacid sequences in **Table S2**). Glycerol dehydrogenase from *Bacillus stearothermophilus* variant L252A (BsGlyDH), ketoreductases from *Neurospora crassa* (NcKRED), *Candida glabratta* (CgKRED), *Bacillus subtitilis* (BsKRED), *Lactobacillus kefir* (LkKRED), NOX from *Lactobacillus pentosus* (LpNOX) and *Thermus thermophilus* (TtNOX), were expressed in *E. coli* BL21 cells. First, 2 mL of Luria Bertani (LB) were inoculated with BL21 cells from a -80°C glycerol backup, in the presence of 30 μg mL^{-1} of kanamycin. After 16 h, 1 mL of media was transferred to a 50 mL Erlenmeyer flask, incubated at 37 °C, and orbital shaking at 250 rpm until 0.6 absorbance units at

600 nm (1 cm optical path) were reached. Afterward, 1 mM (final) concentration of IPTG was added and next incubated at 21 °C overnight for NcKRED, CgKRED, BsKRED, LkKRED, and LpNOX, or 3 h at 37 °C for BsGlyDH and TtNOX. Cells were harvested after centrifugation at 8000 xg for 30 min, and the recovered pellet was resuspended in 5 mL of lysate buffer. (Buffer phosphate 25 mM pH 7.0 for BsGlyDH, LpNOX, and TtNOX; and buffer phosphate 50 mM pH 7.0 + 500 mM NaCl for all KREDs). Cells were broken using a Sonopuls Serie 4200, Bandelin, at 40% amplitude in periods of 3 s followed by 5 s of rest, during 20 min at 4 °C. Lysate was centrifuged at 20,000 x g during 20 min at 4 °C to withdraw the non-soluble matter. The crude extract of all enzymes, except for TtNOX, was purified using metal affinity chromatography.

TtNOx was first partially purified by heat shock, its crude extract was incubated at 70 ºC for 120 min. Afterward, precipitated proteins were removed by centrifugation at 20000 x g for 20 min at 4º C. Uppernatant was used directly for enzyme immobilization.

Purification of enzymes by immobilized metal affinity chromatography (IMAC).

His-tag affinity purification was performed employing Cobalt-activated agarose microbeads 6BCL as support. 5 mL of enzymatic extract was incubated for 1 h at 4 °C with rotatory stirring in the presence of 0.5 g of support previously equilibrated with a lysate buffer, which is specific for each enzyme (see above). After incubation, the support was washed with 2 volumes of lysate buffer, and finally, the enzyme was desorbed by incubating the washed support with lysate buffer with 300 mM of imidazole, for 1 h at 4 °C. Purified extract was centrifuged at 20000 x g for 20 min and filtrated using 0.20 µm syringe filter units. When necessary, imidazole was removed by diafiltration employing 10 kDa Amicon centrifugal filters. The crude extract was reduced to one tenth of its volume and then resuspended to its original volume with a lysate buffer. The process

was completed after 3 cycles (1000 dilution factor). The purified soluble enzymes were saved for later use at 4 °C.

Glycerol dehydrogenase activity.

200 µL of reaction mix containing 100 mM ethyl glyceryl ethers and 1 mM NAD^+ in 50 mM potassium phosphate at pH 7.0 were incubated with 5-10 µL of free enzyme or immobilized biocatalyst suspension at 30 °C. The increment of absorbance at 340 nm due to the reduction of NAD^+ derived from the oxidation of the substrate ethyl glyceryl ether, was monitored using an Epoch microplate reader (CA, USA) with readings every 10 s under continuous agitation. One unit of activity was defined as the amount of enzyme required to reduce 1 µmol of NAD^+ per minute at the assayed conditions. Complementary, glycerol dehydrogenase inhibition assays were performed in the presence of either 0.1-5 mM DHA or EHK. The initial rate was calculated and relativized to calculate the IC_{50} of both products.

Ketoreductase activity

200 µL of reaction mix containing 100 mM of EHK and 0.5 mM NADPH in 50 mM potassium phosphate at pH 7.0 were incubated with 5-10 µL of free enzyme or immobilized biocatalyst suspension at 30 °C. The decrease of absorbance at 340 nm due to the oxidation of NADPH derived from the reduction of the hydroxyketones, was monitored using an Epoch microplate reader (CA, USA), with readings every 10 s with continuous agitation. One unit of activity was defined as the amount of enzyme that was required to oxidize 1 µmol of NADPH per minute at the assayed conditions.

NADH oxidase activity.

200 µL of reaction mix containing 0.5 mM of NADH and 0.15 mM of FAD^+ in 50 mM potassium phosphate at pH 7.0 were incubated with 5-10 µL of free enzyme or immobilized biocatalyst

suspension at 30 °C. The decrease in the absorbance at 340 nm was monitored using an Epoch microplate reader (CA, USA), with readings every 10 s with continuous agitation. One unit of activity was defined as the amount of enzyme that was required to oxidize 1 μmol of NADH per minute at the assayed conditions.[24]

Catalase activity

Catalase (CAT) activity was determined by measuring the decrease in absorbance at 240 nm and 30 °C of a 200 μL solution of 50 mM phosphate buffer pH 7.0 containing 35 mM of H_2O_2. The reaction was started by adding 5-10 μL of free enzyme or immobilized biocatalyst suspension at 30 °C. One unit of CAT activity was defined as the amount of enzyme required for the disproportionation of one μmol of hydrogen peroxide per minute.

Enzyme immobilization by metal affinity interaction.

Similarly, to enzyme purification, immobilization was performed employing Cobalt-activated agarose microbeads 6BCL as support. Specific amounts of protein were offered per mass of support, ranging from 5-60 mg g^{-1} of support in the specific equilibration buffer (lysate buffer, see above). 5 mL of previously purified enzyme solution at the needed concentration were placed in a 10 mL filter column,mixed with 500 mg of previously equilibrated support, and incubated for 1 h at room temperature. After incubation, the immobilized biocatalyst was washed with 2 volumes of equilibration buffer and stored at 4 °C for further use.

When competitive immobilization was required to locate enzymes at the inner surface of the support particles, 100 mM of imidazole was added to the enzyme solution before contacting it with the support. Then, such enzyme solution was incubated with the support overnight. The biocatalyst then was washed with 2 volumes of equilibration buffer and stored at 4° C for further use.

Catalase immobilization in agarose support functionalized with glyoxyl groups.

A solution of commercial bovine liver catalase (CAT) at 10 mg mL^{-1} in buffer 100 mM sodium bicarbonate at pH 10 was incubated for 3–4 h at 4°C with prefabricated agarose beads functionalized with glyoxyl groups in ratio 1:10 (p/v).[38] Afterward, the supernatant was discarded and replaced with 1 mg mL^{-1} of sodium borohydride in buffer 100 mM sodium bicarbonate at pH 10 and incubated for 30 min at 4 ºC. Finally, the heterogeneous biocatalyst was washed with 5 volumes of buffer phosphates 25 mM at pH 7.0 and stored at 4 ºC for further use.

Enzyme labeling and Confocal Laser Scanning Microscopy

Selected enzymes were labeled with fluorophores to evaluate their spatial organization across the agarose bead through fluorescence microscopy. BsGlyDH was labeled with fluorescein isothiocyanate and KRED with ATTO 390 NHS. Briefly, a molar ratio enzyme: fluorophore of 1:1 was placed in buffer sodium bicarbonate 100 mM at pH 9.0 and incubated for 2 h. The unreacted fluorophore was removed by diafiltration using a 10 kDa amicon membrane. Afterwards, enzymes were immobilized as previously detailed in the immobilization methodology section.

Intraparticle protein organization was evaluated employing a suspension of 1:200 of agarose in 25 mM potassium phosphate buffer pH 7.0. The spatial distribution of the enzyme across the agarose support was analyzed using a ZEISS confocal microscope LSM880 with $\lambda ex = 405$ nm, $\lambda ex = 488$ for ATTO 390 NHS, and fluorescein respectively. Images were processed with the software FIJI.[39, 40] Enzyme density was calculated using enzyme penetration data from CLSM and calculated elsewhere.[41]

Deracemization of ethyl and alkyl glyceryl ethers.

0.5 mL of a mixture of 25 mM of ethyl (or alkyl) glyceryl ether, NAD^+ 1 mM, NADPH 0.5 mM, FAD^+ 150 µM, TtNOX and Catalase (activity ratio 1:10: 1000 U, concerning GlyDH activity), 15 % isopropanol in potassium phosphate buffer 25 mM pH 7.0, was added to 100-200 mg different heterogeneous biocatalysts. This biocatalyst load means 1 to 2 mg of enzyme mass per reaction unless stated otherwise. The reaction mixture was incubated at room temperature and stirred in a vertical rotating shaker at 40 rpm. The reaction course was monitored at 2, 4, 8, 12, 24, 48, 72, 96, and 120 h (unless stated differently in the results section) by withdrawing 30 µL of the reaction mixture. For the reaction employing immobilized LpNOX, the free TtNOX/catalase pair was not added, and volumes were substituted with water.

Amplex Red assay for indirect monitoring of the production of NADH

Amplex Red (9-acetyl resorufin) oxidation to Resorufin was coupled to the deracemization reaction to monitor NADH production. The H_2O_2 formed stoichiometrically from the NADH oxidation catalyzed by TtNOx is utilized by horse radish peroxidase to oxidize Amplex red and produce Resorufin (**Scheme S1**).[34, 42] For this assay, the deracemization reaction setup was placed in a 96-well microplate in the absence of catalase to avoid the decomposition of H_2O_2. 0.05 mM of AmplexRed final concentration was added to the mix as well as HRP at 0.5 µg mL^{-1}. Production of resorufin was monitored at 587 nm using an Epoch microplate spectrophotometer (Biotek)

Chromatography sample preparation.

30 µL of the sample were placed in a 1.5 mL microtube and then mixed with 30 µL of methyl imidazole and 225 µL of acetic anhydride. The mixture was incubated at room temperature for 10 min. Next, 300 µL of water was added to quench the reaction, followed by the addition of 300 µL

of dichloromethane with 2 mM of eicosane (internal standard) to extract the derivatized compounds. The mixture was vigorously shaken in a vortex for 30 s, and centrifugated at 15000 x g for 1 min. The bottom phase (organic) was withdrawn and placed into another microtube containing magnesium sulfate to dry the solvent. Then, the organic phase was shaken vigorously in a vortex and centrifuged at 15000 x g for 2 min, the liquid phase was transferred into a 150 µL glass cone inserted in a glass vial for further gas chromatography analysis.

Conventional and chiral gas chromatography.

Samples prepared as described above were analyzed by gas chromatography (GC), employing the Agilent 8890 system, using a column of (5%-phenyl) methylpolysiloxane (Agilent, J&W HP-5 30 m × 0.32 mm × 25 µm), helium as a carrier gas, and equipped with a flame ionization detector (FID). The temperature of the injector and FID detector were 280 and 300 °C, respectively. The separation of compounds was done by the following temperature program: initial temperature 60 °C, maintained 2 min, two ramps, first to 160 °C at a rate of 10 °C min^{-1} and finally to 240 °C at a rate of 20 °C min^{-1}.

Chiral chromatography was performed using a column of β-cyclodextrin in SPB-35 poly (35% phenyl/ 65% dimethylsiloxane phase (BETA DEX TM 120 Capillary column, 30 m x .25 mm x 0.25 µm). Separation of compounds was done by the following temperature ramp: initial temperature 60 °C, two ramps, first to 150 °C at a rate of 2 °C min^{-1}, and finally to 200 °C at a rate of 20 °C min^{-1}. Retention times for all compounds analyzed with this technique are described in **Table S3**.

HPLC chiral chromatography.

Compound Ph00 was analyzed by HPLC (Agilent Infinity 1260 II) with a column Lux i-Amylose-3 chiral (150 x 4.6 mm) Phenomenex, equipped with a DAD detector at 270 nm. The compound

was eluted at a flux of 1 mL min^{-1} using an isocratic method employing a mobile phase of 0.1% TEA in acetonitrile. Retention times were: (*R*)-Ph00: 2.67 and (*S*)-Ph00: 2.93 min

AUTHOR INFORMATION

Corresponding Author

Fernando López-Gallego−Center for Cooperative Research in Biomaterials (CIC biomaGUNE) - Basque Research and Technology Alliance (BRTA), 20014 Donostia- San Sebastián, Spain; IKERBASQUE, Basque Foundation for Science, 48013 Bilbao, Spain

orcid.org/0000-0003-0031-1880; Email:flopez@cicbiomagune.es

Authors

Daniel Grajales-Hernández−Center for Cooperative Research in Biomaterials (CIC biomaGUNE) -Basque Research and Technology Alliance (BRTA), 20014 Donostia- San Sebastián, Spain

Eleftheria Diamanti−Center for Cooperative Research in Biomaterials (CIC biomaGUNE) - Basque Research and Technology Alliance (BRTA), 20014 Donostia- San Sebastián, Spain

Susana Velasco-Lozano− Instituto de Síntesis Química y Catálisis Homogénea (ISQCH-CSIC), Universidad de Zaragoza, 50009 Zaragoza, Spain. Aragonese Foundation for Research and Development (ARAID), 50018, Zaragoza, Spain.

Elisabet Pires− Instituto de Síntesis Química y Catálisis Homogénea (ISQCH-CSIC), University of Zaragoza, 50009 Zaragoza, Spain.

Author Contributions

F.L.-G. conceptualized and supervised the study. D.G.-H., E.D. S.V.-L., and E. P. conducted the investigation. D.G.-H. curated the data and did the formal analysis. D.G.-H. and F.L.-G. designed the methodology. D.G.-H. and F.L.-G. wrote the manuscript. All authors discussed the results and reviewed the manuscript. All authors have approved the final version of the manuscript.

Funding Sources

This work was supported by the Spanish Agency of Research (AEI) (ref. TED2021-129852B-C21, PID2021-124811OB-I00, PID2021-125762NB-I00) and Aragon Government E37_23 R. This work was partially performed under the Maria de Maeztu Units of Excellence Program from the Spanish State Research Agency Grant MDM-2017-0720.

Notes

The authors declare no competing financial interest.

ASSOCIATED CONTENT

Supporting Information.

Supporting Information is available free of charge. Figures S1−S13, table S1-S3, and scheme 1 contain deracemization reaction courses, IC_{50} determination plots, immobilization parameters, aminoacid sequences of the enzymes used, 1H-NMR spectra, GC and HPLC chromatograms, chromatographic retention times of the products, and reaction schemes from the work presented here (PDF)

ACKNOWLEDGMENTS

D.G.-H. acknowledges to Consejo Nacional de Ciencia y Tecnología (CONACyT) for the granted scholarship under the program EPE 2021. S. Velasco and E. Pires acknowledge Gobierno de Aragón grupo E37_23 R. E. Pires also acknowledges the Spanish Ministerio de Ciencia e Innovación (project number PID2021-125762NB-I00).

ABBREVIATIONS

AGE: Alkyl glyceryl ethers, BsGlyDH: *Bacillus stearothermophilus* Glycerol Dehydrogenase, BsGlyDH-L252A: Variant L252A of the *Bacillus stearothermophilus* Glycerol Dehydrogenase, EGE: Ethyl glyceryl ethers, EHK: Ethyl hydroxyketone or 1-ethoxy-3-hydroxypropan-2-one, NAD^+: oxidized nicotinamide adenine dinucleotide, NADH: reduced nicotinamide adenine dinucleotide, TtNOX: *Thermus thermophilus* NADH oxidase, KRED: Ketoreductase, NcKRED: *Neurospora crassa* ketoreductase, CgKRED: *Candida glabratta* ketoreductase BsKRED: *Bacillus subtilis* ketoreductase LkKRED: *Lactobacillus kefir* ketoreductase, $NAD(P)^+$: oxidized nicotinamide adenine dinucleotide phosphate, NAD(P)H: reduced nicotinamide adenine dinucleotide phosphate CAT: Catalase, MPV: Meerwein–Ponndorf–Verley, AG-Co^{+2}: Agarose 6BCL functionalized with iminodiacetic acid and coordinated with divalent ions of cobalt.
NHS: (N-hydroxysuccinimide) HB1-5: Heterogeneous biocatalysts 1 to 5, *e.e.* : enantiomeric excess, GC-FID: Gas chromatography with Flame ionization detector. TOF: Turnover frequency iPGE: Isopropyl glyceryl ethers. LpNOX: *Lactobacillus pentosus* water forming NADH oxidase, AG-G: Agarose functionalized with glyoxyl groups, IPTG: Isopropyl β-D-1-thiogalactopyranoside, IC_{50}: half Inhibitory concentration. DHA: Dihydroxyacetone, CLSM: Confocal laser scanning microscopy, HRP: Horseradish peroxidase.

REFERENCES

(1) Fryszkowska, A.; Devine, P. N. Biocatalysis in drug discovery and development. *Curr. Opin. Chem. Biol.* **2020**, *55*, 151-160, https://doi.org/10.1016/j.cbpa.2020.01.012

(2) Cuetos, A.; Bisogno, F. R.; Lavandera, I.; Gotor, V. Coupling biocatalysis and click chemistry: one-pot two-step convergent synthesis of enantioenriched 1,2,3-triazole-derived diols. *Chem. Commun.* **2013**, *49*, 2625-2627, 10.1039/c3cc38674k

(3) Schmidt-Dannert, C.; Lopez-Gallego, F. A roadmap for biocatalysis - functional and spatial orchestration of enzyme cascades. *Microb. Biotechnol.* **2016**, *9*, 601-609, 10.1111/1751-7915.12386

(4) Schmidt, S.; Castiglione, K.; Kourist, R. Overcoming the Incompatibility Challenge in Chemoenzymatic and Multi-Catalytic Cascade Reactions. *Chem. Eur. J.* **2018**, *24*, 1755-1768, https://doi.org/10.1002/chem.201703353

(5) Bommarius, A. S.; Paye, M. F. Stabilizing biocatalysts. *Chem. Soc. Rev.* **2013**, *42*, 6534-6565, 10.1039/c3cs60137d

(6) Fernandez-Lafuente, R. Stabilization of multimeric enzymes: Strategies to prevent subunit dissociation. *Enzyme Microb. Technol.* **2009**, *45*, 405-418, https://doi.org/10.1016/j.enzmictec.2009.08.009

(7) Velasco-Lozano, S.; Jackson, E.; Ripoll, M.; Lopez-Gallego, F.; Betancor, L. Stabilization of omega-transaminase from Pseudomonas fluorescens by immobilization techniques. *Int. J. Biol. Macromol.* **2020**, *164*, 4318-4328, 10.1016/j.ijbiomac.2020.09.003

(8) Lopez-Gallego, F.; Betancor, L.; Mateo, C.; Hidalgo, A.; Alonso-Morales, N.; Dellamora-Ortiz, G.; Guisan, J. M.; Fernandez-Lafuente, R. Enzyme stabilization by glutaraldehyde crosslinking of adsorbed proteins on aminated supports. *J. Biotechnol.* **2005**, *119*, 70-75, 10.1016/j.jbiotec.2005.05.021

(9) Bolivar, J. M.; Woodley, J. M.; Fernandez-Lafuente, R. Is enzyme immobilization a mature discipline? Some critical considerations to capitalize on the benefits of immobilization. *Chem. Soc. Rev.* **2022**, *51*, 6251-6290, 10.1039/D2CS00083K

(10) Rocha-Martín, J.; Rivas, B. d. l.; Muñoz, R.; Guisán, J. M.; López-Gallego, F. Rational Co-Immobilization of Bi-Enzyme Cascades on Porous Supports and their Applications in Bio-Redox Reactions with In Situ Recycling of Soluble Cofactors. *ChemCatChem* **2012**, *4*, 1279-1288, 10.1002/cctc.201200146

(11) Benítez-Mateos, A. I.; Huber, C.; Nidetzky, B.; Bolivar, J. M.; López-Gallego, F. Design of the Enzyme–Carrier Interface to Overcome the O 2 and NADH Mass Transfer Limitations of an Immobilized Flavin Oxidase. *ACS Appl. Mater. Interfaces* **2020**, *12*, 56027-56038, 10.1021/acsami.0c17568

(12) Tiritan, M. E.; Pinto, M.; Fernandes, C. Enantioselective Synthesis, Enantiomeric Separations and Chiral Recognition. *Molecules* **2020**, *25*, 1713,

(13) Musa, M. M.; Hollmann, F.; Mutti, F. G. Synthesis of enantiomerically pure alcohols and amines via biocatalytic deracemisation methods. *Catal. Sci. Tech.* **2019**, *9*, 5487-5503, 10.1039/c9cy01539f

(14) Voss, C. V.; Gruber, C. C.; Faber, K.; Knaus, T.; Macheroux, P.; Kroutil, W. Orchestration of Concurrent Oxidation and Reduction Cycles for Stereoinversion and Deracemisation of sec-Alcohols. *J. Am. Chem. Soc.* **2008**, *130*, 13969-13972, 10.1021/ja804816a

(15) Peng, T.; Tian, J.; Zhao, Y.; Jiang, X.; Cheng, X.; Deng, G.; Zhang, Q.; Wang, Z.; Yang, J.; Chen, Y. Multienzyme Redox System with Cofactor Regeneration for Cyclic Deracemization of Sulfoxides. *Angew. Chem. Int. Ed.* **2022**, *61*, e202209272, https://doi.org/10.1002/anie.202209272

(16) Li, B.; Nie, Y.; Mu, X. Q.; Xu, Y. De novo construction of multi-enzyme system for one-pot deracemization of (R,S)-1-phenyl-1,2-ethanediol by stereoinversion of (S)-enantiomer to the corresponding counterpart. *J. Mol. Catal. B: Enzym.* **2016**, *129*, 21-28, https://doi.org/10.1016/j.molcatb.2016.04.003
(17) Leal-Duaso, A.; Caballero, M.; Urriolabeitia, A.; Mayoral, J. A.; Garcia, J. I.; Pires, E. Synthesis of 3-alkoxypropan-1,2-diols from glycidol: experimental and theoretical studies for the optimization of the synthesis of glycerol derived solvents. *Green Chem.* **2017**, *19*, 4176-4185, 10.1039/C7GC01583F
(18) Velasco-Lozano, S.; Roca, M.; Leal-Duaso, A.; Mayoral, J. A.; Pires, E.; Moliner, V.; López-Gallego, F. Selective oxidation of alkyl and aryl glyceryl monoethers catalysed by an engineered and immobilised glycerol dehydrogenase. *Chem. Sci.* **2020**, *11*, 12009-12020, 10.1039/d0sc04471g
(19) Bolivar, J. M.; Hidalgo, A.; Sanchez-Ruiloba, L.; Berenguer, J.; Guisan, J. M.; Lopez-Gallego, F.; Sánchez-Ruiloba, L.; Berenguer, J.; Guisán, J. M.; López-Gallego, F. Modulation of the distribution of small proteins within porous matrixes by smart-control of the immobilization rate. *J. Biotechnol.* **2011**, *155*, 412-420, 10.1016/j.jbiotec.2011.07.039
(20) Richter, N.; Hummel, W. Biochemical characterisation of a NADPH-dependent carbonyl reductase from Neurospora crassa reducing α- and β-keto esters. *Enzyme Microb. Technol.* **2011**, *48*, 472-479, https://doi.org/10.1016/j.enzmictec.2011.02.004
(21) Ma, H.; Yang, L.; Ni, Y.; Zhang, J.; Li, C.-X.; Zheng, G.-W.; Yang, H.; Xu, J.-H. Stereospecific Reduction of Methyl o-Chlorobenzoylformate at 300 g·L−1 without Additional Cofactor using a Carbonyl Reductase Mined from Candida glabrata. *Adv. Synth. Catal.* **2012**, *354*, 1765-1772, https://doi.org/10.1002/adsc.201100366
(22) Ni, Y.; Li, C. X.; Ma, H. M.; Zhang, J.; Xu, J. H. Biocatalytic properties of a recombinant aldo-keto reductase with broad substrate spectrum and excellent stereoselectivity. *Appl. Microbiol. Biotechnol.* **2011**, *89*, 1111-1118, 10.1007/s00253-010-2941-4
(23) Noey, E. L.; Tibrewal, N.; Jiménez-Osés, G.; Osuna, S.; Park, J.; Bond, C. M.; Cascio, D.; Liang, J.; Zhang, X.; Huisman, G. W.; et al. Origins of stereoselectivity in evolved ketoreductases. *Proc. Natl. Acad. Sci. USA* **2015**, *112*, E7065-E7072, 10.1073/pnas.1507910112
(24) Rocha-Martín, J.; Vega, D.; Bolivar, J. M.; Godoy, C. A.; Hidalgo, A.; Berenguer, J.; Guisán, J. M.; López-Gallego, F. New biotechnological perspectives of a NADH oxidase variant from Thermus thermophilus HB27 as NAD+-recycling enzyme. *BMC Biotechnol.* **2011**, *11*, 101-101, 10.1186/1472-6750-11-101
(25) Rocha-Martin, J.; Acosta, A.; Guisan, J. M.; López-Gallego, F. Immobilizing Systems Biocatalysis for the Selective Oxidation of Glycerol Coupled to In Situ Cofactor Recycling and Hydrogen Peroxide Elimination. *ChemCatChem* **2015**, *7*, 1939-1947, 10.1002/cctc.201500210
(26) Santiago-Arcos, J.; Velasco-Lozano, S.; Diamanti, E.; Cortajarena, A. L.; López-Gallego, F. Immobilization Screening and Characterization of an Alcohol Dehydrogenase and its Application to the Multi-Enzymatic Selective Oxidation of 1,-Omega-Diols. *Front. Catal.* **2021**, *1*, 9, 10.3389/fctls.2021.715075
(27) Klomp, D.; Maschmeyer, T.; Hanefeld, U.; Peters, J. A. Mechanism of Homogeneously and Heterogeneously Catalysed Meerwein–Ponndorf–Verley–Oppenauer Reactions for the Racemisation of Secondary Alcohols. *Chem. Eur. J.* **2004**, *10*, 2088-2093, https://doi.org/10.1002/chem.200305460

(28) Garcia-Galan, C.; Berenguer-Murcia, Á.; Fernandez-Lafuente, R.; Rodrigues, R. C. Potential of Different Enzyme Immobilization Strategies to Improve Enzyme Performance. *Adv. Synth. Catal.* **2011**, *353*, 2885-2904, 10.1002/adsc.201100534
(29) Rocha-Martin, J.; Acosta, A.; Berenguer, J.; Guisan, J. M.; Lopez-Gallego, F. Selective oxidation of glycerol to 1,3-dihydroxyacetone by covalently immobilized glycerol dehydrogenases with higher stability and lower product inhibition. *Bioresour. Technol.* **2014**, *170*, 445-453, 10.1016/j.biortech.2014.07.116
(30) Rosell, C. M.; Fernandez-Lafuente, R.; Guisan, J. M. Modification of Enzyme Properties by the use of Inhibitors During Their Stabilisation by Multipoint Covalent Attachment. *Biocatal. Biotransform.* **1995**, *12*, 67-76, 10.3109/10242429508998152
(31) Tavano, O. L.; Fernandez-Lafuente, R.; Goulart, A. J.; Monti, R. Optimization of the immobilization of sweet potato amylase using glutaraldehyde-agarose support. Characterization of the immobilized enzyme. *Process Biochem.* **2013**, *48*, 1054-1058, https://doi.org/10.1016/j.procbio.2013.05.009
(32) Casati, S.; Santaniello, E.; Ciuffreda, P. Enzymatic synthesis of both enantiomeric forms of 3-allyloxy-propane-1,2-diol. *Tetrahedron: Asymmetry* **2012**, *23*, 395-400, https://doi.org/10.1016/j.tetasy.2012.03.008
(33) Jiang, R.; Bommarius, A. S. Hydrogen peroxide-producing NADH oxidase (nox-1) from Lactococcus lactis. *Tetrahedron: Asymmetry* **2004**, *15*, 10.1016/j.tetasy.2004.07.057
(34) Mishin, V.; Gray, J. P.; Heck, D. E.; Laskin, D. L.; Laskin, J. D. Application of the Amplex red/horseradish peroxidase assay to measure hydrogen peroxide generation by recombinant microsomal enzymes. *Free Radical Biol. Med.* **2010**, *48*, 1485-1491, https://doi.org/10.1016/j.freeradbiomed.2010.02.030
(35) Kondrat, S.; Krauss, U.; von Lieres, E. Enzyme co-localisation: Mechanisms and benefits. *Curr. Res. Chem. Biol.* **2022**, *2*, 100031, https://doi.org/10.1016/j.crchbi.2022.100031
(36) Nowak, C.; Beer, B.; Pick, A.; Roth, T.; Lommes, P.; Sieber, V. A water-forming NADH oxidase from Lactobacillus pentosus suitable for the regeneration of synthetic biomimetic cofactors. *Front. Microbiol.* **2015**, *6*, 957, 10.3389/fmicb.2015.00957
(37) Prier, C. K.; Camacho Soto, K.; Forstater, J. H.; Kuhl, N.; Kuethe, J. T.; Cheung-Lee, W. L.; Di Maso, M. J.; Eberle, C. M.; Grosser, S. T.; Ho, H.-I.; et al. Amination of a Green Solvent via Immobilized Biocatalysis for the Synthesis of Nemtabrutinib. *ACS Catal.* **2023**, 7707-7714, 10.1021/acscatal.3c00941
(38) Guisán, J. Aldehyde-agarose gels as activated supports for immobilization-stabilization of enzymes. *Enzyme Microb. Technol.* **1988**, *10*, 10.1016/0141-0229(88)90018-x
(39) Diamanti, E.; Arana-Peña, S.; Ramos-Cabrer, P.; Comino, N.; Carballares, D.; Fernandez-Lafuente, R.; López-Gallego, F. Intraparticle Macromolecular Migration Alters the Structure and Function of Proteins Reversibly Immobilized on Porous Microbeads. *Adv. Mater. Interf.* **2022**, *9*, 10.1002/admi.202200263
(40) Diamanti, E.; Santiago-Arcos, J.; Grajales-Hernández, D.; Czarnievicz, N.; Comino, N.; Llarena, I.; Di Silvio, D.; Cortajarena, A. L.; López-Gallego, F. Intraparticle Kinetics Unveil Crowding and Enzyme Distribution Effects on the Performance of Cofactor-Dependent Heterogeneous Biocatalysts. *ACS Catal.* **2021**, *11*, 15051-15067, 10.1021/acscatal.1c03760
(41) Velasco-Lozano, S.; Santiago-Arcos, J.; Mayoral, J. A.; López-Gallego, F. Co-immobilization and Colocalization of Multi-Enzyme Systems for the Cell-Free Biosynthesis of Aminoalcohols. *ChemCatChem* **2020**, *12*, 3030-3041, https://doi.org/10.1002/cctc.201902404

(42) Zhou, M.; Diwu, Z.; Panchuk-Voloshina, N.; Haugland, R. P. A stable nonfluorescent derivative of resorufin for the fluorometric determination of trace hydrogen peroxide: Applications in detecting the activity of phagocyte NADPH oxidase and other oxidases. *Anal. Biochem.* **1997**, *253*, 162-168, 10.1006/abio.1997.2391